Controlling rovibrational state populations of polar molecules in inhomogeneous electric fields of the Stark deceleration: molecular dynamics and quantum chemistry simulations

Emil Zak,[1,*] Jochen Küpper,[1,2,3] and Andrey Yachmenev[1,†]

[1] *Center for Free-Electron Laser Science, Deutsches Elektronen-Synchrotron DESY, Notkestrasse 85, 22607 Hamburg, Germany*
[2] *The Hamburg Center for Ultrafast Imaging, Universität Hamburg, Luruper Chaussee 149, 22761 Hamburg, Germany*
[3] *Department of Physics, Universität Hamburg, Luruper Chaussee 149, 22761 Hamburg, Germany*

(Dated: June 12, 2025)

We propose a modified Stark-chirped rapid adiabatic passage technique for a robust rovibrational population transfer in the gas phase molecules in the presence of certain inhomogeneous electric fields. As an example application, the new state switching scheme is shown to greatly enhance the process of slowing polar ammonia molecules in the Stark decelerator. High-level quantum mechanical simulations show that a virtually complete population inversion between a selected pair of weak-field and strong-field seeking states of NH_3 can be achieved. Strong dc electric fields within the Stark decelerator are used as part of the rovibrational population transfer protocol. Classical-dynamics simulations for ammonia demonstrate notable improvements in the longitudinal phase space acceptance of the Stark decelerator upgraded with the state switching and an increased deceleration efficiency with respect to the standard Stark deceleration technique.

I. INTRODUCTION

Robust control of rotational-vibrational (rovibrational) state populations in the gas phase molecules brings a number of applications, ranging from quantum state-selection [1, 2] for fundamental physics studies, enhanced lasing [3] or implementation of quantum gates [4], to mention few.

A coherent population transfer between a pair of rovibrational states can be achieved with near unit efficiency by the Stark-chirped rapid adiabatic passage (SCRAP) technique [2, 5, 6]. Originally, SCRAP implements two time-delayed Gaussian pulses that partly overlap in time: A pump pulse with a fixed frequency is tuned slightly away from the resonance with the transition of interest. A relatively intense far-off-resonance Stark pulse is used to chirp the transition frequency through the resonance. Here we propose a modification of the SCRAP method, in which the role of the Stark pulse is taken by the dc electric fields present in the system of interest. We demonstrate how the population switching can greatly enhance the process of slowing polar molecules, on the example of the Stark decelerator [7–12]. Yet the scheme presented here is designed to have applications ranging beyond the Stark deceleration technique.

Stark deceleration [7–12] is a popular modern approach to cold-molecules experiments [13–20], where it is used for accelerating, decelerating, and guiding packets of state-selected small polar molecules. The operation principle of Stark deceleration is illustrated in Fig. 1b. The inhomogeneous electric field, produced by voltage differences between pairs of opposing electrodes, creates an effective Stark potential for polar molecules. For molecules in a weak-field seeking (WFS) internal state, the potential energy increases along the molecular beam axis. It reaches the maximum at the position of the maximum field strength, i.e., between the electrodes. Molecules moving in the direction of electrodes climb the potential hill and, therefore, loose kinetic energy. At a moment before molecules reach the position of maximum electric field, the voltages are quickly switched. This prevents molecules from regaining their kinetic energy on the downward slope of the Stark potential. Instead, they have to climb the next hill. This process is repeated by letting the molecules pass through multiple electric field stages.

Conversely, molecules in a strong-field seeking (SFS) state exhibit a Stark potential that has a form of a well

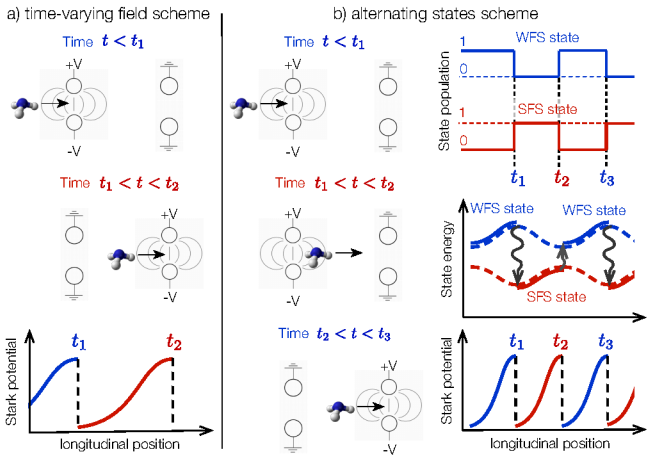

FIG. 1. Stark potential energy of polar molecules as a function of the longitudinal position along the molecular beam axis through the electrode pairs. An effective moving potential wall is created in front of molecular beam by (a) repeated switching of the voltages between field configurations at times t_1 and t_2 or (b) repeated altering of the molecular quantum state between selected SFS and WFS states at times t_1, t_2 and t_3 and corresponding switching of voltages between field configurations at times $t_1, t_2, t_3, \ldots$

* emil@beit.tech; Current affiliation: BEIT Inc., Mogilska 43, 31-545 Kraków, Poland
† andrey.yachmenev@robochimps.com

with its minimum energy at the position of the maximum electric field. Therefore, molecules will gain the kinetic energy when moving in the direction of increasing electric field (toward electrodes) and loose it when going away. In principle, such molecules can be also focused and decelerated by appropriately switched fields [21–28].

One may think of switching the population from one quantum state to another at the points of minimum and maximum of the electric field, such that the effective Stark potential is always upwards-sloped in the direction of the molecular motion. In this way, molecules will continually loose their kinetic energy on both the upward and downward slopes of the electric field, which is illustrated in Fig. 1b. A seemingly similar idea to Stark deceleration has been theoretically proposed in [29], yet there are a number of key differences discussed in section II which make the present technique more robust and more practical. Sisyphus opto-electrical cooling method [30, 31] is also based on a similar idea to produce ultra-cold molecules. Very recently, a concept of state switching with adiabatic-passage techniques has been utilized [32] to control the excition qubit dynamics in quantum dots.

In the Stark decelerator, the field switching sequence is calculated with the help of a hypothetical synchronous molecule moving along the molecular beam axis. The fields are switched every time the synchronous molecule reaches a certain position with respect to the electrodes, expressed in terms of a phase angle $\phi_0 = 0 \ldots 90\,^\circ$. The limiting values 0 and $90\,^\circ$ correspond to the points of minimum and maximum of electric field along the beam axis. The phase angle is always chosen slightly away from the position of the field maximum ($\phi_0 \approx 80\,^\circ$) in order to increase the phase space, i.e., velocity and position, acceptance of molecules along the molecular beam axis. The exact value of the phase angle is calculated depending on the initial position and velocity distribution of molecules and the desired final velocity. In the transverse directions, molecules in WFS states are focused towards the molecular beam axis, resulting in time-dependent transverse oscillatory trajectories of molecules around the synchronous molecule.

In the alternating states (AS) Stark deceleration method, see Fig. 1, the electric field configuration is switched at $\phi_0 \approx 0$, while the population is transferred back and forth between the WFS and SFS states at $\phi_0 \approx 0$ and $90\,^\circ$. The transverse focusing mechanism is similar to that in the alternating gradient decelerator [24], except the fact that molecules are focused toward the beam center in WFS state and defocused away in the SFS state moving along the same transverse direction and within one electric field stage.

Besides Stark deceleration, several other techniques for producing slow molecular beams have been advanced in the recent years, such as buffer-gas cooling [33, 34], direct laser cooling [35, 36], Sisyphus [30, 31, 37], sympathetic [38], or evaporative [39] cooling, and photoassociation of ultracold atoms [40, 41]. Many of these techniques can benefit from using the Stark decelerator as a preceding stage [42] for producing high intensities of cold beams in selected rovibrational states from a wide range of polar molecular species.

Here, we explore the idea of altering the internal state of the whole ensemble of molecules in the molecular beam in the presence of inhomogeneous electric fields. As an example we show how this method help to improve the efficiency and the phase-space characteristics of the Stark deceleration method. We propose and theoretically validate a robust method for population inversion between a pair of SFS and WFS states of a molecule, based on the rapid-adiabatic passage with a Stark-shift chirp produced by the controlled time-modulation of the electric field in Stark decelerator. Applied to a beam of ammonia ($^{14}NH_3$) molecules, the proposed method shows 2-3 times larger longitudinal velocity acceptance than the conventional decelerator resulting in higher final densities of cold molecules. Furthermore, since molecules are slowed down on both upward and downward slopes of the electric field, the number of mechanical deceleration stages, required to reach a desired final velocity, can be reduced by a factor of two. This aids the deceleration of heavy or less polar molecules at lower field strengths. The present method could be implemented using one of the existing Stark decelerators by mounting an additional laser source and fast semiconductor voltage switches.

II. POPULATION INVERSION IN THE STARK DECELERATOR

A coherent population transfer between a pair of WFS and SFS rovibrational states can be produced with a very high efficiency by the Stark-chirped rapid adiabatic passage (SCRAP) technique [2, 5, 6]. The standard SCRAP implements two time-delayed Gaussian pulses that partly overlap in time: A pump pulse with a fixed frequency ω_p is tuned slightly away from the resonance with the WFS-to-SFS transition $\Delta E_{\rm res}$. A relatively intense far-off-resonance Stark pulse is used to chirp the transition frequency $\Delta E_{\rm res} + \Delta_{\rm S}(t)$ through the resonance with $\hbar\omega_p$ by inducing a dynamic Stark shift $\Delta_{\rm S}(t)$. The SCRAP population transfer is robust to fluctuations in the intensities of the pulses, as long as other parameters – such as the pump frequency, and the delay time – are carefully controlled.

It is therefore essential that there are no further strong detunings present in the system, e.g., inhomogeneous broadenings of transition frequency or external electric fields. Such perturbations can significantly lower the percentage of the population transfer, which represents a major obstacle for employing SCRAP within the Stark decelerator. Although the highly spatially inhomogeneous electric field aids the deceleration, it induces an additional static detuning of the transition frequency, i.e., $\Delta E_{\rm res} + \Delta_{\rm dc}(\vec{r})$, which depends on the position of the molecule $\vec{r}$ in the decelerator. As a result, SCRAP will produce a complete population inversion only for a frac-

tion of the total amount of molecules, which have an appropriate dc Stark shift, i.e., only for molecules located within certain confined regions in the decelerator. This would, for example, demand two different sets of the Stark and pump pulses to be employed for the population inversion at the areas of minimum and maximum of the electric field. However, the principal problem is that the variation in the dc field detuning over a typical spatial-acceptance region of the decelerator is much larger than the detuning normally produced by a Stark pulse, i.e., $|\Delta_{\rm dc}(\vec{r'}) - \Delta_{\rm dc}(\vec{r})| \gg \Delta_{\rm S}(t)$. Nonetheless, increasing the Stark pulse intensity, i.e., increasing $\Delta_{\rm S}(t)$, would make the population transfer more sensitive to the intensity fluctuations in the pump pulse. One can try to make $\Delta_{\rm dc}(\vec{r}) = 0$, i.e., switch off the dc electric field for a short period of time, i.e., a fraction of a microsecond, and carry out the SCRAP population inversion. This, however, may lead to the so-called Majorana transitions into the non-polarizable molecular states, e.g., states with $m = 0$, and correspondingly to a significant loss of molecular density. Another option would be to create a dc electric field that is uniform in the longitudinal and transverse directions, i.e., $\Delta_{\rm dc}(\vec{r}) = {\rm const.}$, which is, however, technically very challenging; it could possibly be implemented in a Stark decelerator with large-flat-area electrodes [29].

Here, we develop an alternative scheme to circumvent this problem by using a temporally controlled rise of the dc electric field in decelerator to produce the rapid-adiabatic passage transfer. The second Stark pulse of the original SCRAP is discarded and the operation scheme can be described as follows: when molecules reach a position where their population has to be transferred between SFS and WFS states, see Fig. 1, the voltages $V(t)$ are first dropped to $V_{\rm min}$ as in the conventional Stark decelerator. Then the pump field (ω_p) is turned on and the voltages $V(t)$ are ramped up to $V_{\rm max}$ in a time of about 0.1–0.2 μs ($V_{\rm min} \le V(t) \le V_{\rm max}$). The applied voltages generate the time- and position-dependent dc electric field, which in turn produces the spatially inhomogeneous Stark shift of the transition frequency $\Delta_{\rm dc}(\vec{r}, t)$ in molecules. The minimal and the maximal voltages are chosen such that by varying $V(t)$ over a period of time $t = 0 \ldots t_{\rm max}$, the condition

$$\Delta E_{\rm res} + \Delta_{\rm dc}(\vec{r}, t_{\rm res}) = \hbar\omega_p \qquad (1)$$

is satisfied at some resonance time $0 < t_{\rm res} < t_{\rm max}$ for every position $\vec{r}$ within a large acceptance-volume inside the decelerator. The sufficiently intense pump field, applied during the resonance crossing, produces a complete adiabatic passage of population from initial to final states [6]. The adiabatic evolution of the population is ensured by a smooth temporal rise of the voltages, a long interaction time, and a strong electric dipole coupling between the interacting states. When the voltages reach the operating value $V_{\rm max}$, the pump field is turned off and molecules continue into the next deceleration stage. In ref. [29] a seemingly similar idea of WFS/SFS population switching has been proposed, however there are some key differences. Firstly, in [29] two laser pulses: Stark pulse and pump pulse are required. Secondly, ref. [29] uses stimulated Raman adiabatic-passage method to switch between strong-field seeking and weak-field seeking states, whereas we use Stark-Chirped rapid-adiabatic passage (SCRAP) method. A disadvantage of STIRAP is that its efficiency in transferring populations between rovibrational states is sensitive to inhomogeneous broadening of respective energy levels [2]. To the contrary, our Stark-chirped rapid-adiabatic-passage method *utilizes* the Stark-shifts to rovibrational energy levels as a means of sweeping through resonance with the pump-field frequency. In this way, there is a reasonably large margin for energy dispersion of the initial/final state.

We simulate the SCRAP population transfer in the molecule by solving the corresponding time-dependent Schrödinger equation and calculating the time-dependent probabilities for finding the molecule in the SFS or WFS state. Specifically, the objective is to optimize the time-dependent voltage function $V(t)$ that would maximize the efficiency of the population transfer between selected rovibrational states. For these simulations we choose the prototypical ammonia ($^{14}NH_3$) molecule. The lowest-energy state of para-ammonia is the rotational state $|J, k, m\rangle = |1, 1, 1\rangle$ of the vibronic ground state. This state is split by $\Delta E_{a-s} = 0.794$ cm^{-1} due to the inversion tunneling into the symmetric $E_s = 16.173$ cm^{-1} and the antisymmetric $E_a = 16.967$ cm^{-1} component. These components have opposite parity and repel each other in the presence of an external electric field, producing a pair of closely lying SFS and WFS states. To model the dc electric field produced by the Stark decelerator we picked a conventional electrode configuration. Each stage of the decelerator is formed by two parallel cylindrical electrodes of diameter 3 mm, with their axes parallel to either x or y, and their surfaces separated by 2 mm. The distance between the centers of two stages is 6 mm along the molecular beam axis z, and successive stages are rotated through 90° about the z axis. When voltage is applied to electrodes along the x axis, the electrodes along the y axis are grounded and vice versa, such that the electric field vector is always contained in the xz or yz planes. Since the electric field is periodic and symmetric, for simulations we choose a unit cell $z = [z_{\rm min}, z_{\rm max}]$ between the centers of two neighbouring stages, where the electrodes at $z_{\rm min}$ are grounded and the voltage is applied to the electrodes at $z_{\rm max}$. The resulting dc electric field is computed on a dense grid using a finite elements approach [43]. The maximal value of the applied voltage was set to $|V_{\rm max}| = 10$ kV, which creates an electric field of 1.9 kV/cm, 23.2 kV/cm, and 91.1 kV/cm at $z_{\rm min}$, $(z_{\rm min} + z_{\rm max})/2$, and $z_{\rm max}$, respectively, along the molecular beam axis through the electrode pairs.

To simplify the analysis of the time-dependent probabilities in terms of the SFS and WFS state populations, the minimal voltage was set to zero, $V_{\rm min} = 0$, at the end of SCRAP simulation. In the actual Stark deceleration experiment, however, the electric field is never let

below 300 V/cm to avoid Majorana transitions into the non-polarized $m = 0$ states [44].

The voltage raise over a time of $t_{\max}$ is modelled by the function

$$V(t) = N^{-1} \ln\left(\frac{1 + e^{-a(t_{\max}-t)}}{1 + e^{-at_{\max}}}\right)(V_{\max} - V_{\min}) + V_{\min} \tag{2}$$

where the value of the parameter a is to be optimized and $N = \ln(2/(1 + e^{-at_{\max}}))$ is the normalization factor. For the present simulations we choose $t_{\max} = 130$ ns. The pump field

$$E_p(t) = \begin{cases} \frac{1}{1+e^{-0.4t+8}} E_0 \cos\omega_p t & \text{for } t \le t_{\max}, \\ 0 & \text{otherwise,} \end{cases} \tag{3}$$

is characterized by the frequency $\hbar\omega_p = 0.797$ cm^{-1}, linear polarization along the main direction of the electric field, i.e., x or y for different stages, the peak intensity of $E_0 = 300$ V/cm, and the duration of $t_{\max}$. To ensure the adiabatic evolution of the time-dependent probabilities, the pump pulse time profile is modelled by a quasi-step function with a smooth sigmoid-shape rise extended over 20 ns. The time evolution of the dc field, generated by the voltage function in (2), together with the pump field $E_p(t)$, are plotted in the top panel of Fig. 2, where the voltage rise is delayed by the $E_p(t)$ rising time of 20 ns.

With the use of a full-dimensional spectroscopically refined potential energy surface for ammonia [45], we first variationally obtained the field-free rovibrational energies and wavefunctions for the rotational quantum number $J = 0 \ldots 10$, including all vibrational excitations with band centers below 4000 cm^{-1}. To model the interaction of the molecules with the external electric fields, we used a full-dimensional *ab initio* dipole-moment surface for ammonia [46] and computed all corresponding rovibrational matrix elements of the laboratory-fixed dipole-moment operator using TROVE [47–49] and RichMol [50]. The time-dependent wavepacket exposed by interactions with the electric fields was modelled as a linear combination of the field-free rovibrational states with time-dependent coefficients. The latter were obtained from numerical solution of the time-dependent Schrödinger equation (TDSE) [50]. The initial wavepacket was given by either symmetric or antisymmetric $|1, 1, 1\rangle$ stationary (field-free) state of ammonia.

The populations of different stationary states in the wavepacket are given by the squares of the respective time-dependent coefficients (probabilities). For example, for the position $x, y, z = 0, 0, z_{\max}$ and the voltage rise parameter $a = 0.030$ ns^{-1} the results of numerical simulations are presented in the bottom panel of Fig. 2. The time evolution of the populations of symmetric and antisymmetric $|1, 1, 1\rangle$ states is plotted. The corresponding field configuration is sketched in the upper panel of Fig. 2. At the terminal time $t_{\max} = 150$ ns the dc electric field reaches its maximum and the SCRAP is finished. However, since the dc electric field mixes both the symmetric

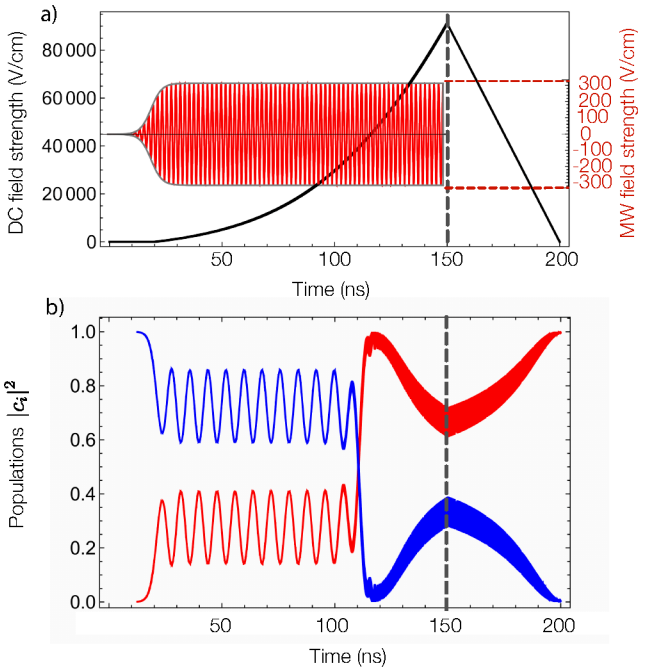

FIG. 2. Top: Temporal evolution of the dc (black) and the microwave-pump (red) electric fields. The dc field corresponds to the position $z = z_{\max}$ and the voltage rise function parameter $a = 0.030$, see (2). Bottom: Temporal evolution of the populations of the symmetric (blue) and antisymmetric (red) $|J, k, m\rangle = |1, 1, 1\rangle$ states of ammonia.

and the antisymmetric state components, it is not possible to exactly quantify the result of the population inversion effect. To work out the populations of the stationary states, we continue to propagate the wavepacket in the presence of the adiabatically decreasing dc electric field (voltage) until it reaches zero at time $t = 200$ ns. By computing the squares of the final coefficients and comparing them to their initial, $t = 0$, values, the population transfer efficiency can be quantified. Fig. 2 shows almost complete population transfer (99.8 %) from symmetric to antisymmetric rovibrational state of ammonia.

To optimize the voltage time rise function in (2), we have performed a series of numerical solutions of the TDSE for different positions z between $z_{\min}$ and $z_{\max}$ and different values of the a parameter. The results of these calculations, shown in Fig. 3, confirm that by appropriately tuning the voltage rise parameter a between 0.030 and 0.070 ns^{-1} one can achieve very high population transfer efficiency, more than 99.5 %, over a wide range of positions z.

The stability of SCRAP with respect to the Stark-shift chirping rate is limited. Since the Stark shifts of selected WFS and SFS energy levels of ammonia behave quadratically at low fields and almost linearly at high fields, different chirping rates must be implemented for molecules located far and near the electrodes, respectively. Optimization of the voltage-rise function has the goal of keeping the chirping rate within the tolerance limit of the

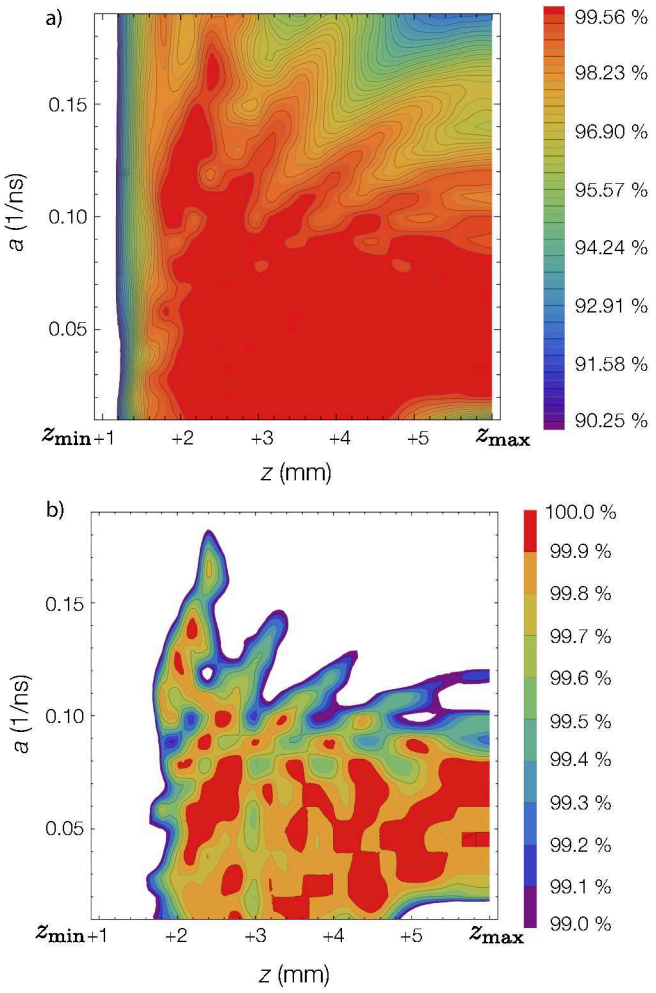

FIG. 3. Contour plots of the target state population (in %) as a function of the voltage time rise parameter a, as defined in (2), and the longitudinal position z along the decelerator axis. Top and bottom plots correspond to population ranges 90-100 % and 99-100 %, respectively.

rapid-adiabatic passage for all locations, ideally within the full acceptance volume of the decelerator.

III. MOLECULAR TRAJECTORY SIMULATIONS

Classical-dynamics simulations of a prototypical Stark-deceleration experiment combined with the alternating states method are employed to calculate molecular trajectories:

$$m\frac{L}{\pi}\ddot{\vec{r}} = \frac{1}{2}\left(W(t)-1\right)\left(\nabla E_{\mathrm{SFS}}(\vec{r}) - \nabla E_{\mathrm{WFS}}(\vec{r})\right) - \nabla E_{\mathrm{WFS}}(\vec{r}) \qquad (4)$$

where $\vec{r}$ is the molecule-trajectory vector, m is the mass of the molecule, and $\nabla E_{\mathrm{WFS}}(\vec{r})$ and $\nabla E_{\mathrm{SFS}}(\vec{r})$ are position dependent gradients of the Stark energies of the WFS and SFS internal molecular states, respectively. $W(t)$ is a time-dependent state occupation function with value $W(t) = 1$ if the molecule is in the WFS state and $W(t) = -1$ if it is in the SFS state. We assume that virtually complete population inversion between WFS and SFS states can be achieved. A theoretical estimate of the losses due to incomplete population inversion is about 0.4 % of the number of trapped molecules per deceleration stage, see Fig. 3.

The Stark energies and gradients for the selected WFS and SFS states of ammonia, i.e., the inversion-split pair of $|J,k,m\rangle = |1,1,1\rangle$ states, are obtained as described above, Sec. II. The position-dependent gradients $\nabla E_{\mathrm{WFS}}(\vec{r})$ and $\nabla E_{\mathrm{SFS}}(\vec{r})$ are calculated for the periodic electric field created by the Stark decelerator with the electrode configuration as described in Sec. II and the peak voltage is set to 10 kV.

The molecule-trajectory vector $\vec{r}$ is defined by two Cartesian coordinates x and y, describing the transverse position of the molecule relative to the molecular beam center, and a phase angle ϕ describing the relative position in the longitudinal direction, i.e., along the molecular beam axis. Since the Stark potential is periodic over two electrode stages, the phase-angle coordinate is defined as $\phi = \pi z/L$ ($\phi = 0 \ldots 2\pi$), where z is Cartesian position along the longitudinal axis, and L is the distance between centers of two neighboring electrode stages. The values of $\phi = n\pi$ and $\phi = n\pi/2$ ($n = 0, 1, 2$) correspond to the points of minimum and maximum of the electric field. The voltage- and state-switching sequence is determined by the choice of the synchronous angle ϕ_0, a value of the phase coordinate ϕ for the central molecule in the beam at the moment the fields or states are switched.

We generate a uniformly-distributed molecule packet in all six dimensions in phase space, with an average forward velocity of 300 m/s, the value typical for pulsed molecular beams [8, 51, 52]. Initial velocity and position spreads of 5 m/s and 2 mm, respectively, in both longitudinal and transverse directions, are reduced with respect to typical pulsed molecular beam experimental values, for the clarity of presentation of phase-space snapshots shown in Fig. 4. We solve (4) numerically for trajectories of 5000 molecules and record their final positions in phase space after 30 deceleration stages; corresponding arrival-time and phase-space distributions are plotted in Fig. 4.

Three different voltage and internal state switching schemes are investigated. In the first scheme, all molecules are initially prepared in the WFS state and only the dc fields in the decelerator are switched, which is equivalent to the standard "alternating gradient" (AG) deceleration method [24, 26]. In the second operation scheme all molecules are initially in the WFS state, the decelerator's fields are kept constant using the peak voltages, and the internal state population of molecules is switched between WFS and SFS states. Similarly to AG, we call this method the "alternating states" (AS) scheme. Notably, in the AS scheme, states are switched two times a deceleration

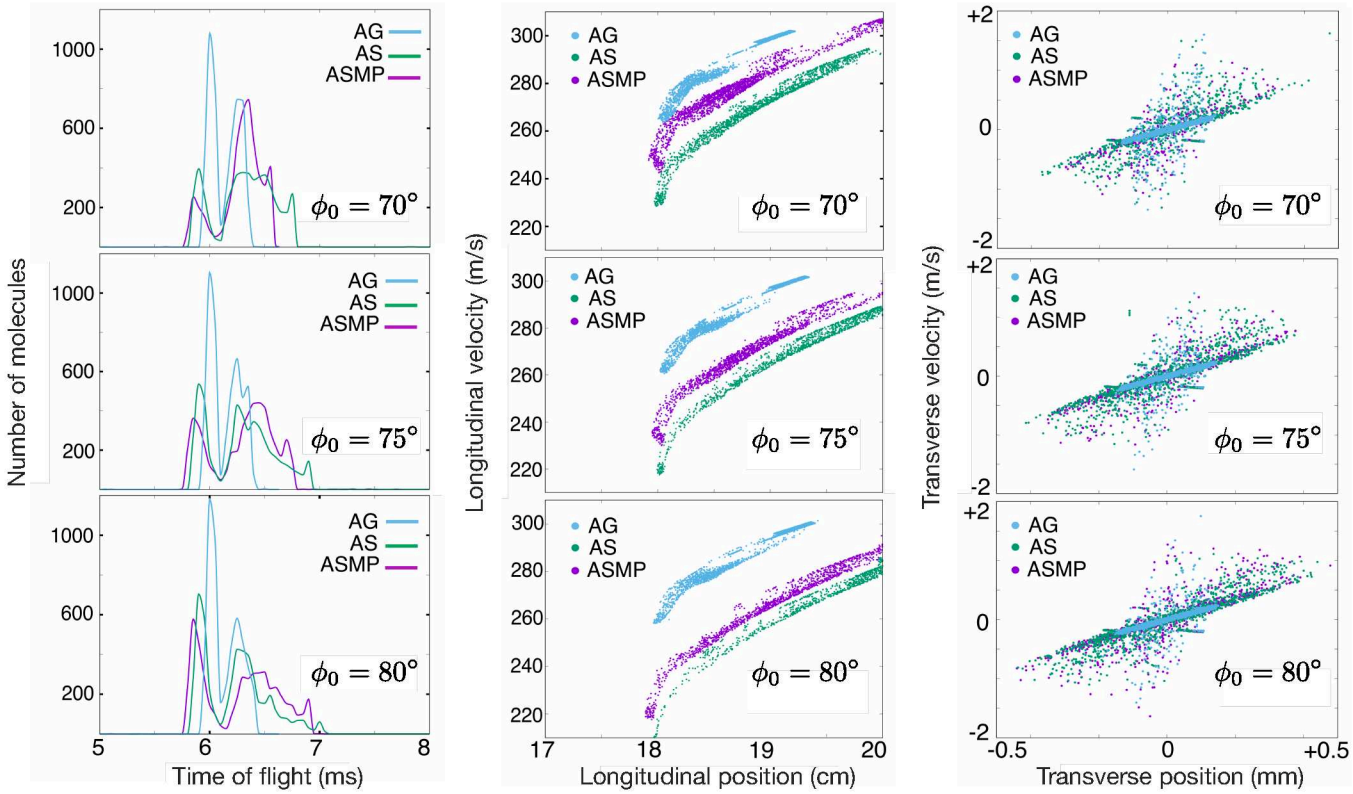

FIG. 4. Calculated time-of-flight profiles and phase-space distributions of NH_3 for ASMP (magenta), AS (green) and AG (blue) deceleration schemes operating at a phase angle $\phi_0 = 70°$, $75°$, and $80°$ with 30 deceleration stages. The transverse position is given by the y-coordinate. A 50 μ bin-size was used in generating time-of-flight histograms.

stage at ϕ_0 and $\phi_0 + \pi/2$, i.e., at the points close to the minimum and the maximum of electric field. The third scheme combines the alternating states approach with the slight modulation of the electrostatic potential (ASMP), which improves the longitudinal acceptance of the method. In this scheme, the voltage on the electrodes is slightly decreased by 2 kV for a period of time between $\phi_0 - \delta$ and ϕ_0, that is before the state switching, and then increased by 4 kV after the state switching, for a period of time between ϕ_0 and $\phi_0 + \delta$, where we chose $\delta = 5°$.

Fig. 4 compares the time-of-flights (TOF) and the phase space acceptance of different schemes for three choices of the phase angle $\phi_0 = 70\,°$, $75\,°$, and $80\,°$. The improvement of the AS and ASMP schemes is clearly visible in the TOF profiles for higher values of the synchronous angle. For $\phi_0 = 80°$, the ASMP peak in the TOF profile at 6.9 ms corresponds to an average final forward velocity of 220 m/s, as shown on the longitudinal phase plot. For comparison, using the same number of deceleration stages, the AG method slows molecules down to an average forward velocity of 260 m/s. The ASMP works best at high values of the phase angle, providing extra longitudinal velocity acceptance however, modulation of the potential in ASMP results in lowered ability to slow molecules. These results are summarized in Table I, which compares the number of deceleration stages needed for the synchronous molecule to reach a given longitudinal velocity (270 m/s and 240 m/s, respectively). The AS scheme requires approximately half of the stages as compared to the AG scheme. The nearly doubled efficiency of the AS technique is a direct consequence of alternating between the WFS and SFS states.

Comparison of molecular packets with equal average velocity (v) for the AG, AS and ASMP methods shows that:

TABLE I. Required number of deceleration stages (N) for AG, AS, and ASMP deceleration schemes, and final molecular number densities for packets slowed down from the initial velocity $v = 300$ m/s to the final velocities $v = 270$ m/s and $v = 240$ m/s. Results are shown for two choices of synchronous angles $\phi_0 = 70°$ and $80°$. Molecular number densities (%mol) are evaluated as fractions of the initial total number of molecules (in percent) with the final longitudinal velocity in the range $v \pm 10$ m/s.

v (m/s)	ϕ_0	AG		AS		ASMP	
		N	%mol	N	%mol	N	%mol
270	70°	27	26	14	51	18	46
	80°	22	24	11	38	13	53
240	70°	50	2	27	9	34	5
	80°	42	1	21	5	24	10

a) the AS and ASMP schemes capture more molecules than AG, hence provide higher molecular densities; b) at synchronous angle $\phi_0 = 80\,^\circ$ the ASMP method gives higher molecular densities than the AS method, i.e., 53 % vs 38 % at $v = 270$ m/s and 10 % vs. 5 % at $v = 240$ m/s. The additional short-time voltage increase in the ASMP method provides an extra focusing force, which when properly timed, guarantees capturing of a larger number of molecules. Further longitudinal slowing of molecules is possible when more deceleration stages are used. At low velocities (< 20 m/s) the phase-stability of the molecular packet decreases rapidly [53], which presents a major challenge to subsequent trapping of the slowed molecules.

The transverse velocity spread shown in the right column in Fig. 4 is similar for all three methods. For $\phi_0 = 80°$ the transverse phase-space diagrams are qualitatively identical. For lower values of the synchronous angle, the spread in the transverse positions for AS and ASMP methods becomes smaller than for AG method. This suggests that due to the effectively shorter focusing and defocusing distances in AS and ASMP, large amplitudes in the transverse motion are produced when the synchronous angle is small, which leads to larger losses of molecular density. A compromise value of ϕ_0 between the transverse and the longitudinal phase space acceptances for AS and ASMP is somewhere in between $70\,^\circ$ and $80\,^\circ$.

IV. CONCLUSIONS

The influence of an induced inversion of the internal-state population of decelerated molecules on the efficiency and the phase-space-acceptance characteristics of the Stark decelerator were studied. Decelerated molecules are switched back and forth between selected WFS and SFS rovibrational states such that the induced Stark potential is pointing upward along the molecular beam axis on both, ascending and descending, branches of the decelerator's electric field. Specifically, we developed and computationally tested a new scheme for population inversion in molecules, based on the rapid adiabatic passage with a Stark-shift chirp created by controlled time-modulation of the electric field in a decelerator. Rigorous quantum-mechanical calculations for ammonia molecule demonstrated a population inversion efficiency larger than 99.5 % for spatially extended, long, molecular beams. Classical trajectory simulations demonstrated the potential of controlling the internal state of decelerated molecules for obtaining a larger phase-space acceptance in the longitudinal direction and more efficient deceleration.

The comprehensive internal-state control presented in this paper also gives new prospects for separating molecules in different hyperfine states, which is important in collision studies and high-precision spectroscopy. Calculations for these purposes can now be made with latest update to the TROVE program [54], which allows for high accuracy rovibrational calculations with nuclear-quadrupole interactions included. Finally, it is interesting to test the present method on slow molecular beams, e.g., in combination with the recently proposed advanced switching operation mode of the Stark decelerator [55].

V. ACKNOWLEDGMENTS

We are grateful to Gabriele Santambrogio, Noah Fitch, and Mike Tarbutt for valuable discussions. This work has been supported by the Deutsche Forschungsgemeinschaft (DFG) through the priority program "Quantum Dynamics in Tailored Intense Fields" (QUTIF, SPP 1840, KU 1527/3, YA 610/1) and through the Clusters of Excellence "Center for Ultrafast Imaging" (CUI, EXC 1074, ID 194651731) and "Advanced Imaging of Matter" (AIM, EXC 2056, ID 390715994).

[1] W. E. Perreault, H. Zhou, N. Mukherjee, and R. N. Zare, Harnessing the power of adiabatic curve crossing to populate the highly vibrationally excited H_2 (v=7,j=0) level, Phys. Rev. Lett. **124**, 163202 (2020).

[2] M. Oberst, H. Münch, G. Grigoryan, and T. Halfmann, Stark-chirped rapid adiabatic passage among a three-state molecular system: Experimental and numerical investigations, Phys. Rev. A **78**, 033409 (2008).

[3] H. Li, E. Lötstedt, H. Li, Y. Zhou, N. Dong, L. Deng, P. Lu, T. Ando, A. Iwasaki, Y. Fu, S. Wang, J. Wu, K. Yamanouchi, and H. Xu, Giant enhancement of air lasing by complete population inversion in N_2^+, Phys. Rev. Lett. **125**, 053201 (2020).

[4] D. Møller, L. B. Madsen, and K. Mølmer, Quantum gates and multiparticle entanglement by rydberg excitation blockade and adiabatic passage, Phys. Rev. Lett. **100**, 170504 (2008).

[5] T. Rickes, L. P. Yatsenko, S. Steuerwald, T. Halfmann, B. W. Shore, N. V. Vitanov, and K. Bergmann, Efficient adiabatic population transfer by two-photon excitation assisted by a laser-induced stark shift, J. Chem. Phys. **113**, 534 (2000).

[6] A. A. Rangelov, N. V. Vitanov, L. P. Yatsenko, B. W. Shore, T. Halfmann, and K. Bergmann, Stark-shift-chirped rapid-adiabatic-passage technique among three states, Phys. Rev. A **72**, 053403 (2005).

[7] H. L. Bethlem, G. Berden, and G. Meijer, Decelerating neutral dipolar molecules, Phys. Rev. Lett. **83**, 1558 (1999).

[8] S. Y. T. van de Meerakker, H. L. Bethlem, and G. Meijer, Taming molecular beams, Nat. Phys. **4**, 595 (2008).

[9] S. A. Meek, H. L. Bethlem, H. Conrad, and M. G., Trapping molecules on a chip in travelling potential wells, Phys. Rev. Lett. **100**, 153003 (2008), arXiv:0801.2943 [physics].

[10] M. T. Bell and T. P. Softley, Ultracold molecules and ultracold chemistry, Mol. Phys. **107**, 99 (2009).

[11] S. D. Hogan, C. Seiler, and F. Merkt, Rydberg-state-enabled deceleration and trapping of cold molecules, Phys.

Rev. Lett. **103**, 123001 (2009).
[12] S. Y. T. van de Meerakker, H. L. Bethlem, N. Vanhaecke, and G. Meijer, Manipulation and control of molecular beams, Chem. Rev. **112**, 4828 (2012).
[13] J. van Veldhoven, J. Küpper, H. L. Bethlem, B. Sartakov, A. J. A. van Roij, and G. Meijer, Decelerated molecular beams for high-resolution spectroscopy: The hyperfine structure of $^{15}ND_3$, Eur. Phys. J. D **31**, 337 (2004).
[14] R. V. Krems, Molecules near absolute zero and external field control of atomic and molecular dynamics, Int. Rev. Phys. Chem. **24**, 99 (2005).
[15] J. J. Gilijamse, S. Hoekstra, S. Y. T. van de Meerakker, G. C. Groenenboom, and G. Meijer, Near-threshold inelastic collisions using molecular beams with a tunable velocity, Science **313**, 1617 (2006).
[16] E. R. Hudson, H. J. Lewandowski, B. C. Sawyer, and J. Ye, Cold molecule spectroscopy for constraining the evolution of the fine structure constant, Phys. Rev. Lett. **96**, 143004 (2006).
[17] M. Schnell and J. Küpper, Tailored molecular samples for precision spectroscopy experiments, Faraday Disc. **150**, 33 (2011).
[18] B. K. Stuhl, M. T. Hummon, and J. Ye, Cold state-selected molecular collisions and reactions, Annu. Rev. Phys. Chem. **65**, 501 (2014).
[19] M. L. Wall, K. Maeda, and L. D. Carr, Realizing unconventional quantum magnetism with symmetric top molecules, New J. Phys. **17**, 025001 (2015).
[20] S. N. Vogels, J. Onvlee, S. Chefdeville, A. van der Avoird, G. C. Groenenboom, and S. Y. T. Meerakker, Imaging resonances in low-energy no-he inelastic collisions., Science **350**, 787 (2015), arXiv:1510.00299 [physics].
[21] D. Auerbach, E. E. A. Bromberg, and L. Wharton, Alternate-gradient focusing of molecular beams, J. Chem. Phys. **45**, 2160 (1966).
[22] H. L. Bethlem, A. J. A. van Roij, R. T. Jongma, and G. Meijer, Alternate gradient focusing and deceleration of a molecular beam, Phys. Rev. Lett. **88**, 133003 (2002).
[23] M. R. Tarbutt, H. L. Bethlem, J. J. Hudson, V. L. Ryabov, V. A. Ryzhov, B. E. Sauer, G. Meijer, and E. A. Hinds, Slowing heavy, ground-state molecules using an alternating gradient decelerator, Phys. Rev. Lett. **92**, 173002 (2004).
[24] H. L. Bethlem, M. R. Tarbutt, J. Küpper, D. Carty, K. Wohlfart, E. A. Hinds, and G. Meijer, Alternating gradient focusing and deceleration of polar molecules, J. Phys. B **39**, R263 (2006), arXiv:0604020 [physics].
[25] K. Wohlfart, F. Grätz, F. Filsinger, H. Haak, G. Meijer, and J. Küpper, Alternating-gradient focusing and deceleration of large molecules, Phys. Rev. A **77**, 031404(R) (2008), arXiv:0803.0650 [physics].
[26] K. Wohlfart, F. Filsinger, F. Grätz, J. Küpper, and G. Meijer, Stark deceleration of OH radicals in low-field-seeking and high-field-seeking quantum states, Phys. Rev. A **78**, 033421 (2008).
[27] F. Filsinger, U. Erlekam, G. von Helden, J. Küpper, and G. Meijer, Selector for structural isomers of neutral molecules, Phys. Rev. Lett. **100**, 133003 (2008), arXiv:0802.2795 [physics].
[28] Y.-P. Chang, D. A. Horke, S. Trippel, and J. Küpper, Spatially-controlled complex molecules and their applications, Int. Rev. Phys. Chem. **34**, 557 (2015), arXiv:1505.05632 [physics].
[29] E. R. Hudson, Deceleration of continuous molecular beams, Phys. Rev. A **79**, 061407 (2009).
[30] M. Zeppenfeld, B. G. U. Englert, R. Glöckner, A. Prehn, M. Mielenz, C. Sommer, L. D. van Buuren, M. Motsch, and G. Rempe, Sisyphus cooling of electrically trapped polyatomic molecules, Nature **491**, 570 (2012), arXiv:1208.0046 [physics].
[31] A. Prehn, M. Ibrügger, R. Glöckner, G. Rempe, and M. Zeppenfeld, Optoelectrical cooling of polar molecules to submillikelvin temperatures, Phys. Rev. Lett. **116**, 063005 (2016), arXiv:1511.09427 [physics].
[32] A. Mukherjee, A. Widhalm, D. Siebert, S. Krehs, N. Sharma, A. Thiede, D. Reuter, J. Förstner, and A. Zrenner, Electrically controlled rapid adiabatic passage in a single quantum dot, Applied Physics Letters **116**, 251103 (2020).
[33] N. R. Hutzler, H.-I. Lu, and J. M. Doyle, The buffer gas beam: An intense, cold, and slow source for atoms and molecules, Chem. Rev. **112**, 4803 (2012), arXiv:1111.2841 [physics].
[34] V. Singh, A. K. Samanta, N. Roth, D. Gusa, T. Ossenbrüggen, I. Rubinsky, D. A. Horke, and J. Küpper, Optimized cell geometry for buffer-gas-cooled molecular-beam sources, Phys. Rev. A **97**, 032704 (2018), arXiv:1801.10586 [physics].
[35] J. Barry, E. Shuman, E. Norrgard, and D. DeMille, Laser radiation pressure slowing of a molecular beam, Phys. Rev. Lett. **108**, 103002 (2012), arXiv:1110.4890 [physics].
[36] S. Truppe, H. J. Williams, N. J. Fitch, M. Hambach, T. E. Wall, E. A. Hinds, B. E. Sauer, and M. R. Tarbutt, An intense, cold, velocity-controlled molecular beam by frequency-chirped laser slowing, New J. Phys. **19**, 022001 (2017), arXiv:1605.06055 [physics].
[37] D. Comparat, Molecular cooling via sisyphus processes, Phys. Rev. A **89**, 043410 (2014), arXiv:1404.2689 [physics].
[38] J. Lim, M. D. Frye, J. M. Hutson, and M. R. Tarbutt, Modeling sympathetic cooling of molecules by ultracold atoms, Phys. Rev. A **92**, 053419 (2015), arXiv:1508.03987 [physics].
[39] B. K. Stuhl, M. T. Hummon, M. Yeo, G. Quéméner, J. L. Bohn, and J. Ye, Evaporative cooling of the dipolar hydroxyl radical, Nature **492**, 396 (2012), arXiv:1209.6343 [physics].
[40] K.-K. Ni, S. Ospelkaus, M. H. G. de Miranda, A. Pe'er, B. Neyenhuis, J. J. Zirbel, S. Kotochigova, P. S. Julienne, D. Jin, and J. Ye, A high phase-space-density gas of polar molecules, Science **322**, 231 (2008).
[41] J. Pérez-Ríos, M. Lepers, and O. Dulieu, Theory of long-range ultracold atom-molecule photoassociation, Phys. Rev. Lett. **115**, 073201 (2015), arXiv:1505.03288 [physics].
[42] C. Cheng, A. P. P. van der Poel, P. Jansen, M. Quintero-Pérez, T. E. Wall, W. Ubachs, and H. L. Bethlem, Molecular fountain, Phys. Rev. Lett. **117**, 253201 (2016), arXiv:1611.03640 [physics].
[43] COMSOL Multiphysics v. 5.5. `http://www.comsol.com`. COMSOL AB, Stockholm, Sweden.
[44] H. L. Bethlem, F. M. H. Crompvoets, R. T. Jongma, S. Y. T. van de Meerakker, and G. Meijer, Deceleration and trapping of ammonia using time-varying electric fields, Phys. Rev. A **65**, 053416 (2002).
[45] S. N. Yurchenko, R. J. Barber, and J. Tennyson, A variationally computed line list for hot NH_3, Mon. Not. R. Astron. Soc. **413**, 1828 (2011), arXiv:1011.1569 [astro-ph].

[46] S. N. Yurchenko, R. J. Barber, A. Yachmenev, W. Thiel, P. Jensen, and J. Tennyson, A variationally computed $T = 300$ K line list for NH_3, J. Phys. Chem. A **113**, 11845 (2009).

[47] S. N. Yurchenko, W. Thiel, and P. Jensen, Theoretical ROVibrational energies (TROVE): A robust numerical approach to the calculation of rovibrational energies for polyatomic molecules, J. Mol. Spectrosc. **245**, 126 (2007).

[48] A. Yachmenev and S. N. Yurchenko, Automatic differentiation method for numerical construction of the rotational-vibrational Hamiltonian as a power series in the curvilinear internal coordinates using the Eckart frame, J. Chem. Phys. **143**, 014105 (2015).

[49] S. N. Yurchenko, A. Yachmenev, and R. I. Ovsyannikov, Symmetry adapted ro-vibrational basis functions for variational nuclear motion calculations: TROVE approach, J. Chem. Theory Comput. **13**, 4368 (2017), arXiv:1708.07185 [physics].

[50] A. Owens and A. Yachmenev, RichMol: A general variational approach for rovibrational molecular dynamics in external electric fields, J. Chem. Phys. **148**, 124102 (2018), arXiv:1802.07603 [physics].

[51] G. Scoles, ed., *Atomic and molecular beam methods*, Vol. 1 (Oxford University Press, New York, NY, USA, 1988).

[52] W. Christen, K. Rademann, and U. Even, Supersonic beams at high particle densities: Model description beyond the ideal gas approximation, J. Phys. Chem. A **114**, 11189 (2010).

[53] M. Schnell and G. Meijer, Cold molecules: Preparation, applications, and challenges, Angew. Chem. Int. Ed. **48**, 6010 (2009).

[54] A. Yachmenev and J. Küpper, Communication: General variational approach to nuclear-quadrupole coupling in rovibrational spectra of polyatomic molecules, J. Chem. Phys. **147**, 141101 (2017), arXiv:1709.08558 [physics].

[55] D. Zhang, G. Meijer, and N. Vanhaecke, Advanced switching schemes in a Stark decelerator, Phys. Rev. A **93**, 023408 (2016), arXiv:1512.08361 [physics].